

Supporting Information

Lithium intercalation mechanisms and critical role of multi-doping in $\text{LiFe}_x\text{Mn}_{2-x-y}\text{Ti}_y\text{O}_4$ as high-capacity cathode material for Lithium-ion batteries

D. Callegari¹, M. Coduri¹, M. Fracchia¹, P. Ghigna¹, L. Braglia², U. Anselmi Tamburini¹ and E. Quartarone^{1,*}

¹*Department of Chemistry and INSTM-GISEL, University of Pavia, Via Taramelli 16 27100 Pavia, Italy*

²*CNR - Istituto Officina dei Materiali, TASC, I-34149 Trieste, Italy*

**Corresponding author: eliana.quartarone@unipv.it*

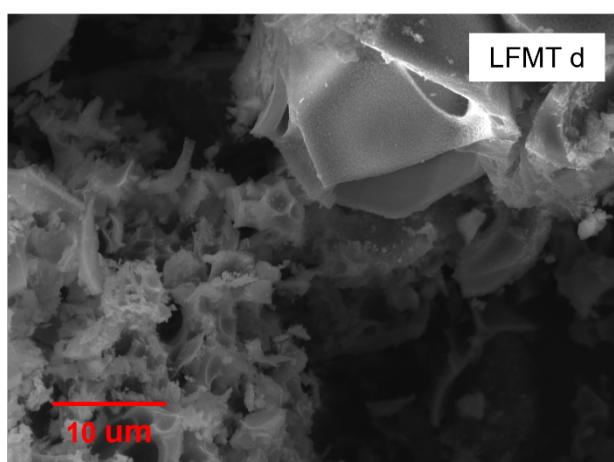
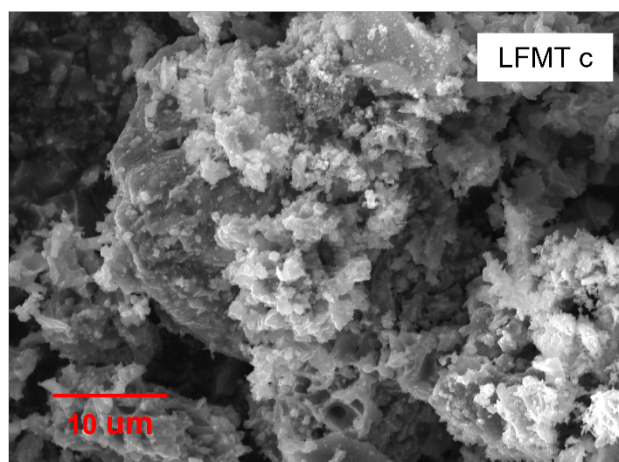
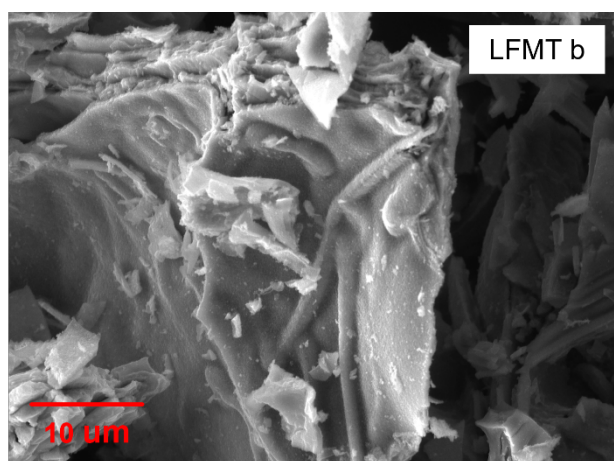
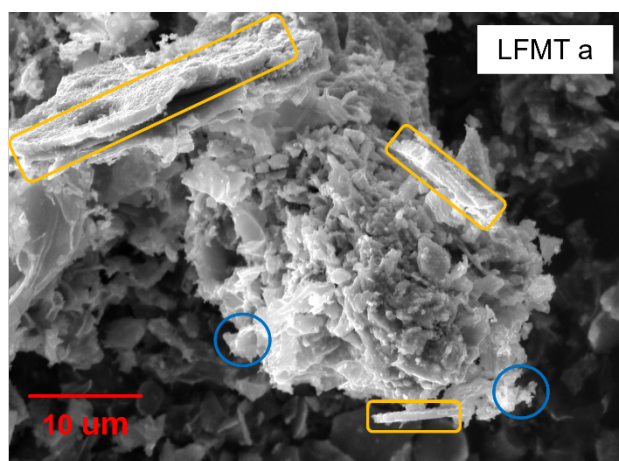


Figure S1: SEM image of the pristine LFMT sample prepared via sol–gel route and calcination at low temperature

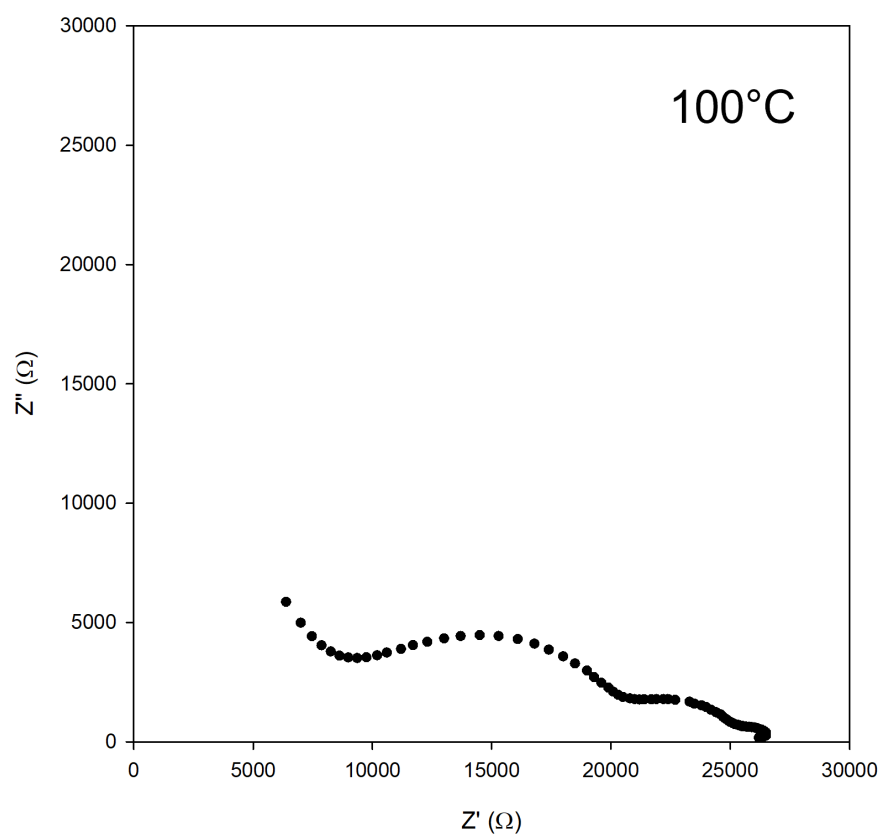


Figure S2(I): Impedance spectrum of a LFMT c pellet, recorded/obtained at 100°C

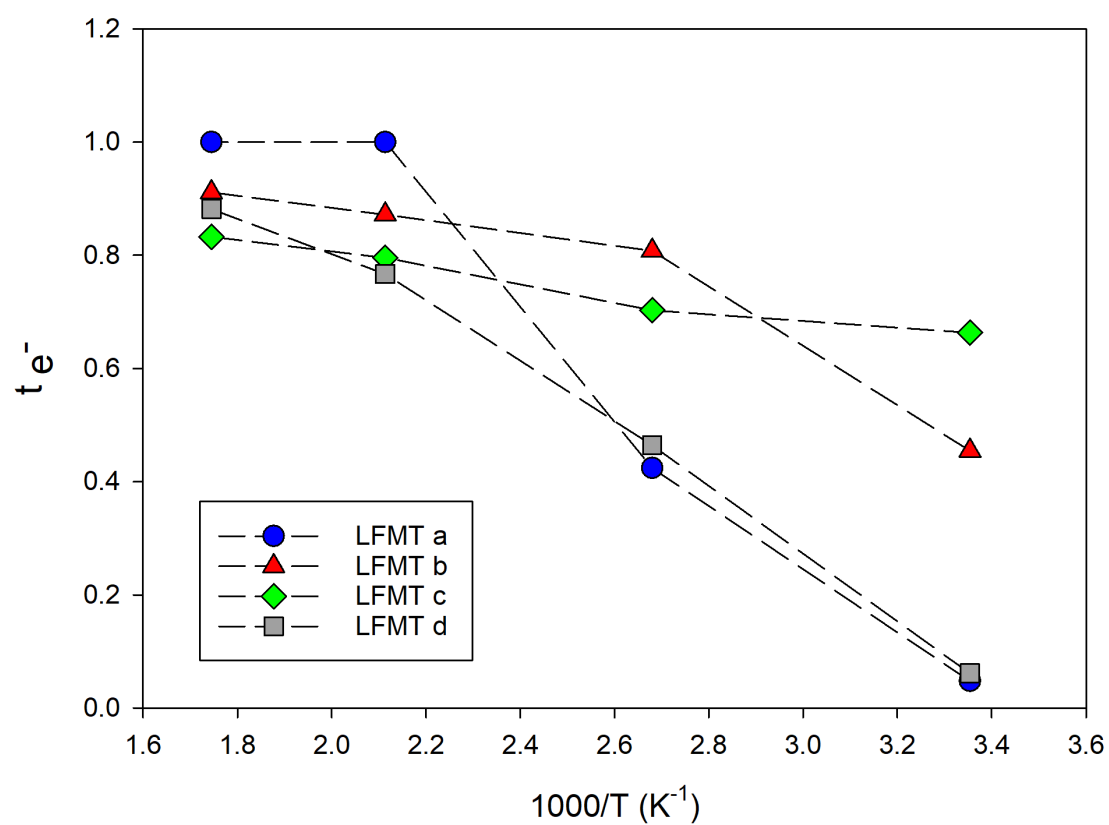


Figure S2(II): Electron transference numbers, t_e^- , vs T, as calculated by the respective Nyquist plots

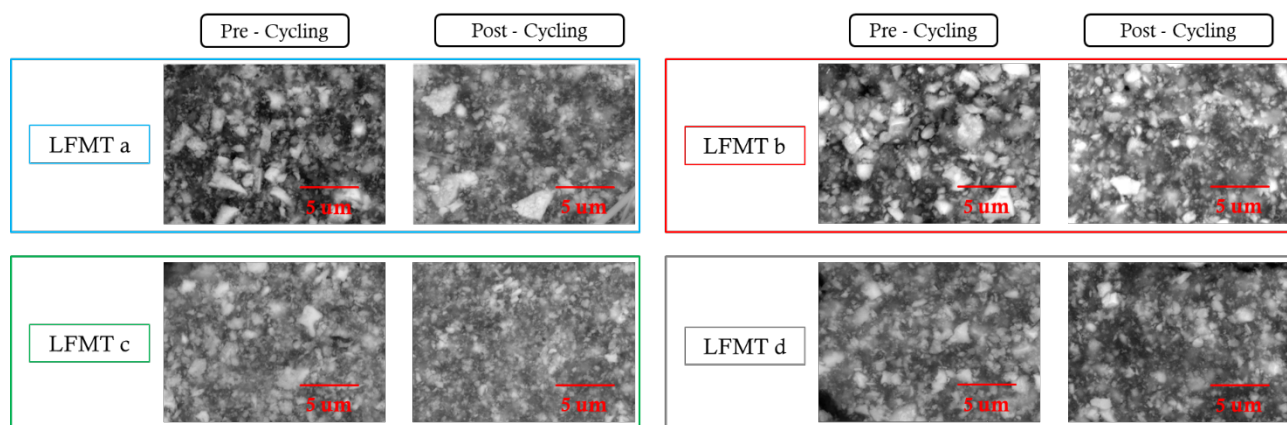


Figure S3(I): (Back-scattered) SEM images of the LFMT electrodes pre- and post-cycling

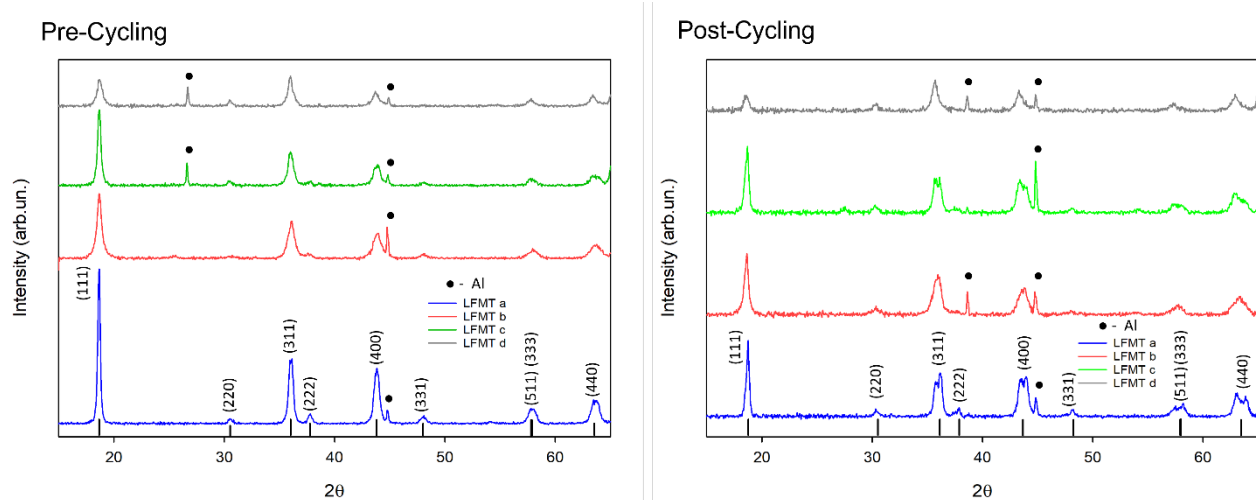


Figure S3(II): XRD patterns of the pre-cycled (left) and post-cycled LFMT electrodes (right). The star • in plots indicates the Al signal coming from the current collector.

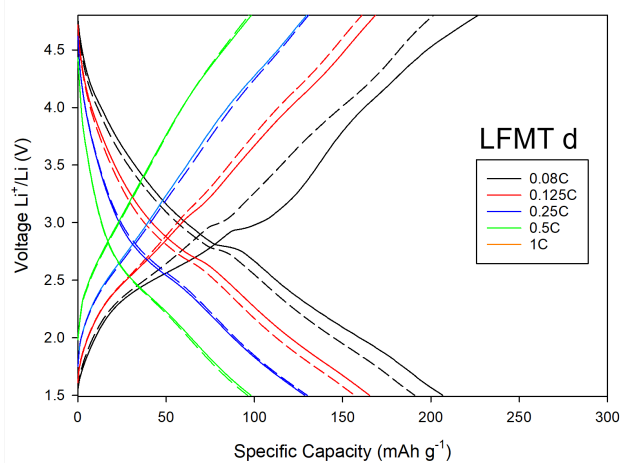
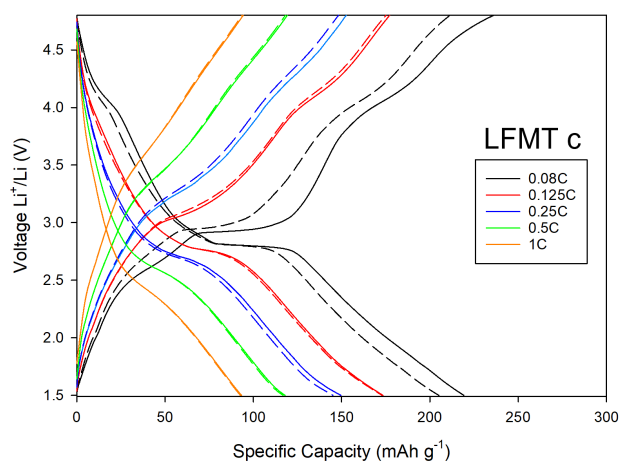
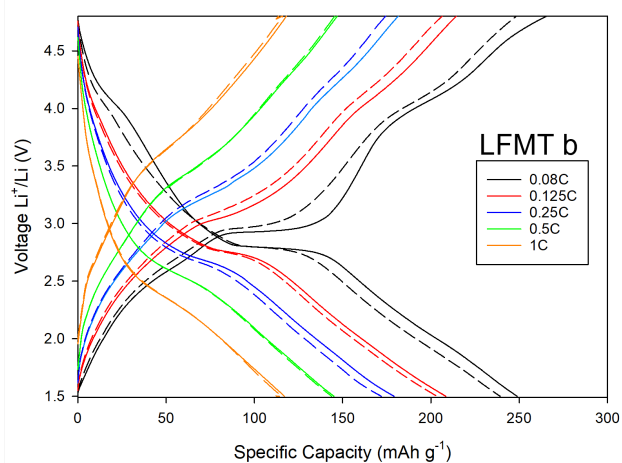
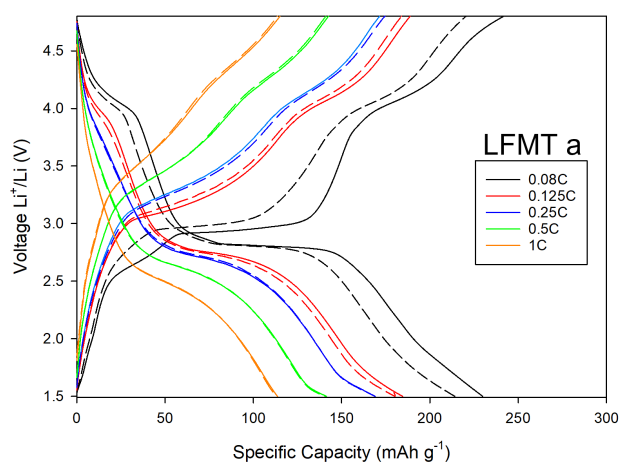


Figure S4: Voltage profiles of the 2nd (solid line) and 5th (dotted line) cycles at each investigated C_{rate} .

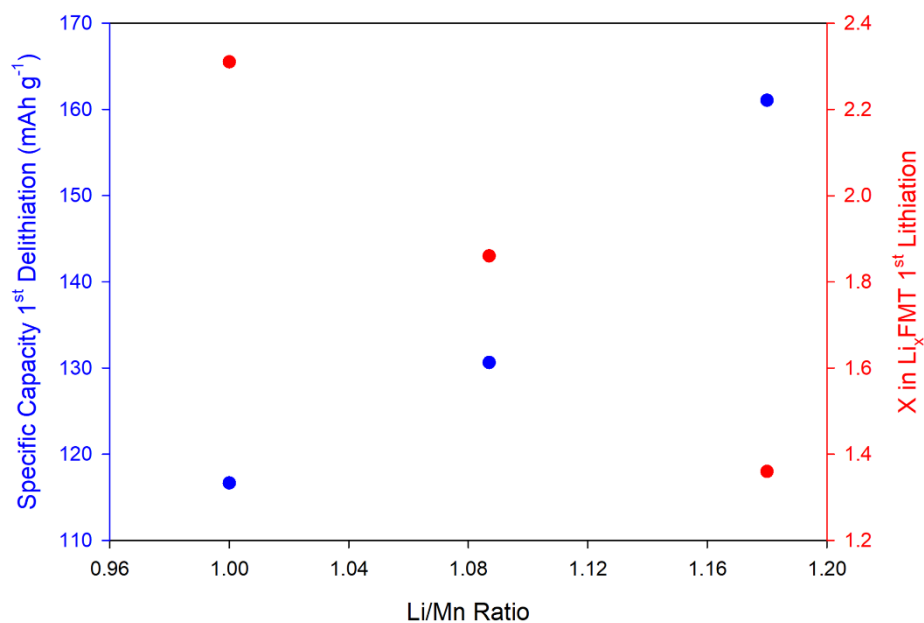


Figure S5(I): 1st Delithiation Capacity (blue) and Lithium stoichiometry, x , (red) as a function of the Li/Mn molar ratio in LFMTa-d cathodes.

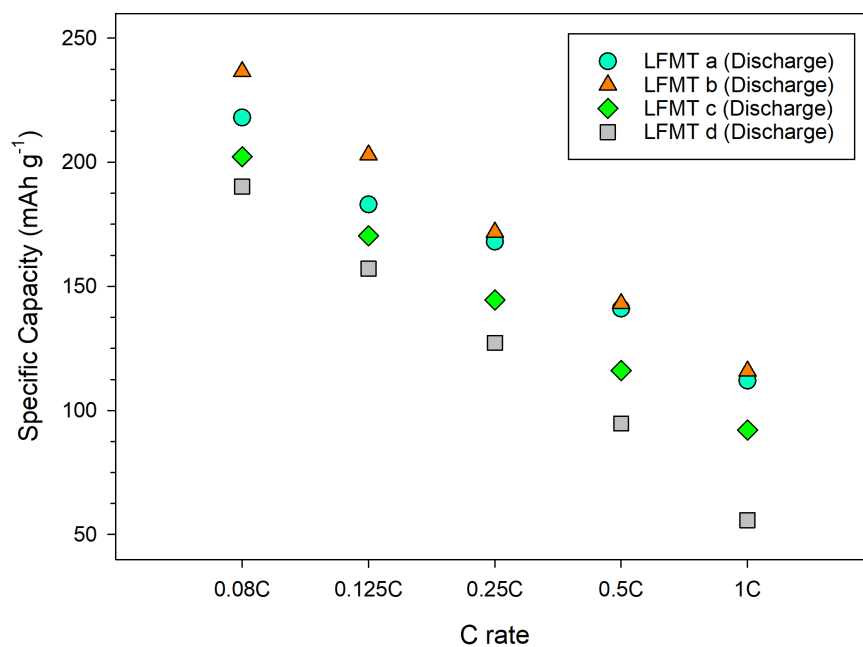


Figure S5(II): Discharge Capacity behavior as a function of C_{rate} in LFMTa-d cathodes.

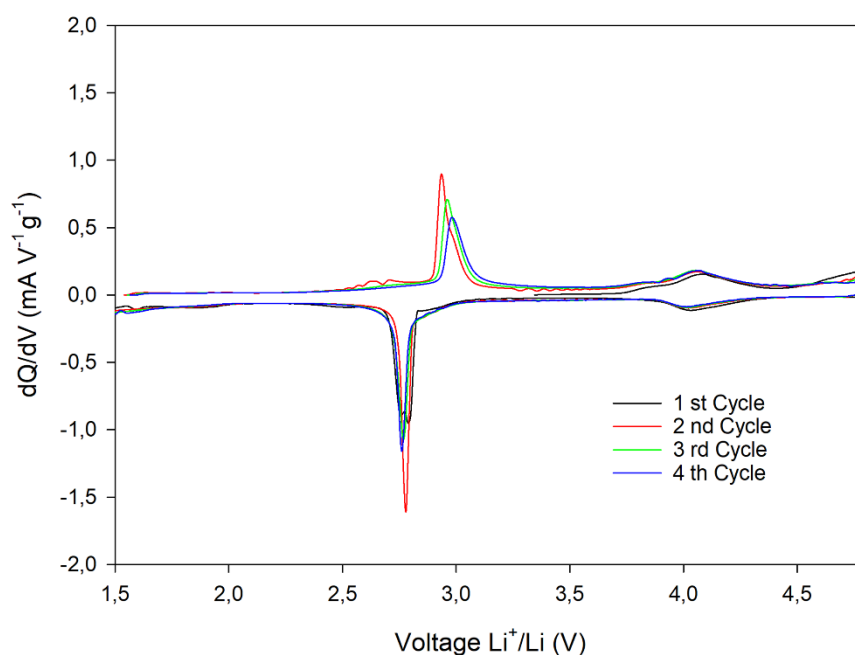


Figure S6(I): dQ/dV plots of LFMTa cathode with LP30 + 4% (wt%) of Succinic Anhydride as electrolyte

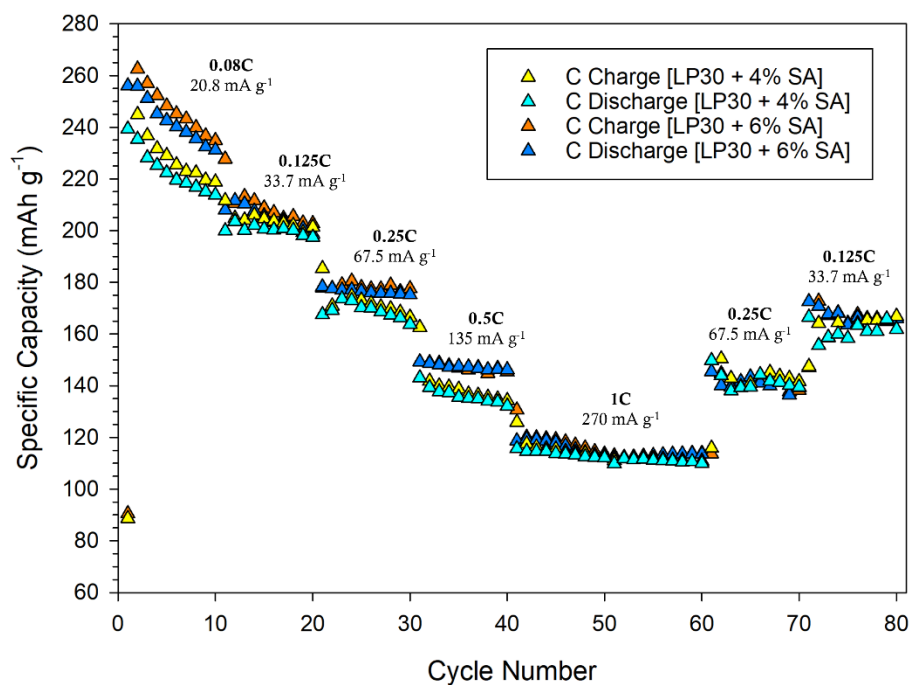


Figure S6(II): Galvanostatic cycling at different C_{Rate} of the cell LFMTa/electrolyte/Li. Electrolyte: $LiPF_6$ 1.0M in EC/DMC (1/1 v/v) + 4% (cyano/yellow) and 6% (wt %) (blue/red) of Succinic Anhydride.

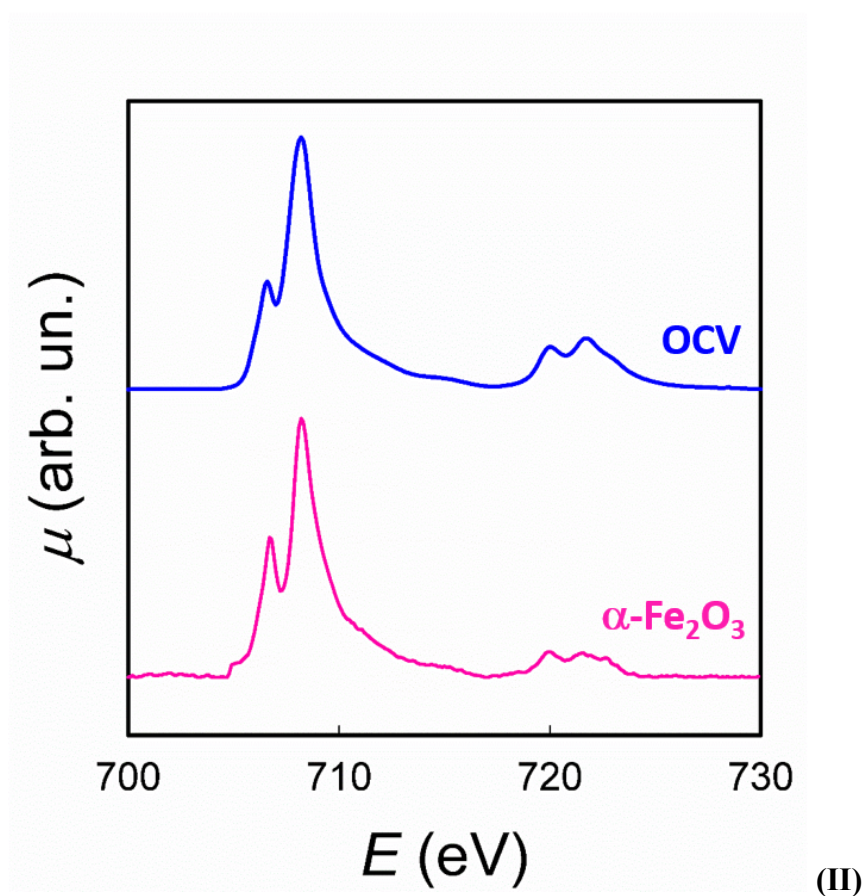
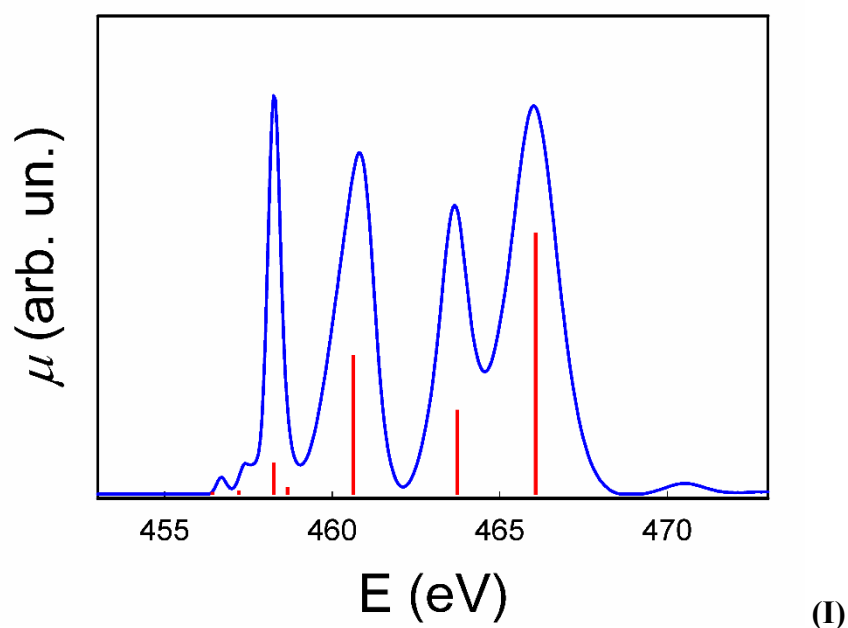
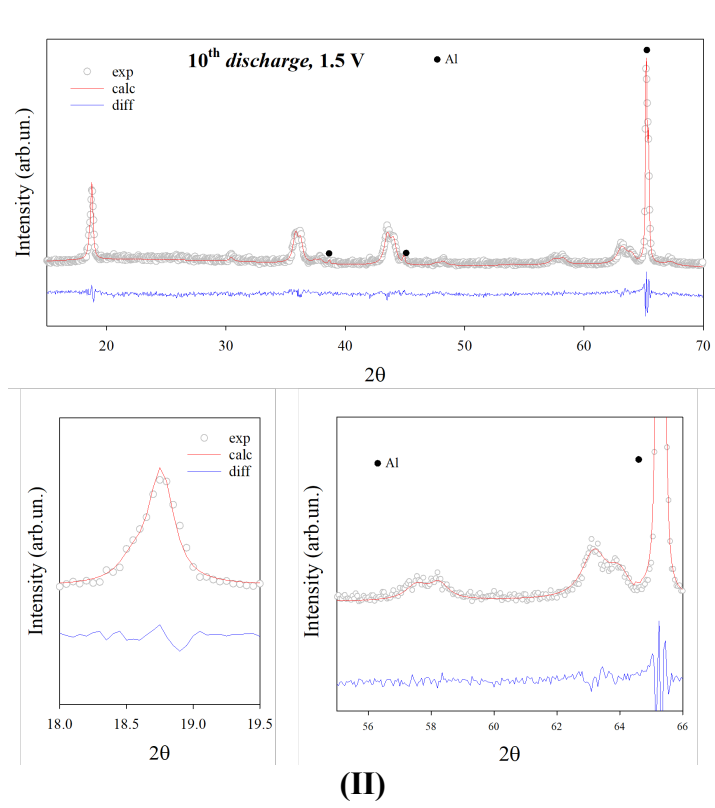
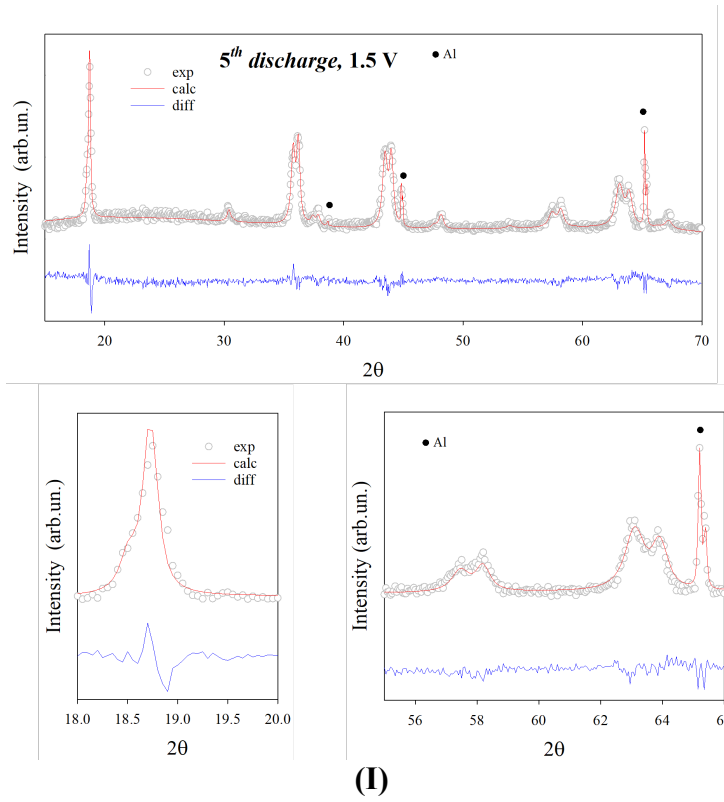


Figure S7: (I) Ti $L_{2,3}$ -edges of sample LFMTc at OCV (blue line). The red bars are the multiplets calculated by means of the XTM4XAS program¹, including crystal field, charge transfer, and spin-orbit coupling effects and assuming Ti in Oh environment; (II) XANES spectra at the Fe $L_{2,3}$ -edges of LFMTc at OCV (blue line) and $\alpha\text{-Fe}_2\text{O}_3$ (pink line), taken as reference.



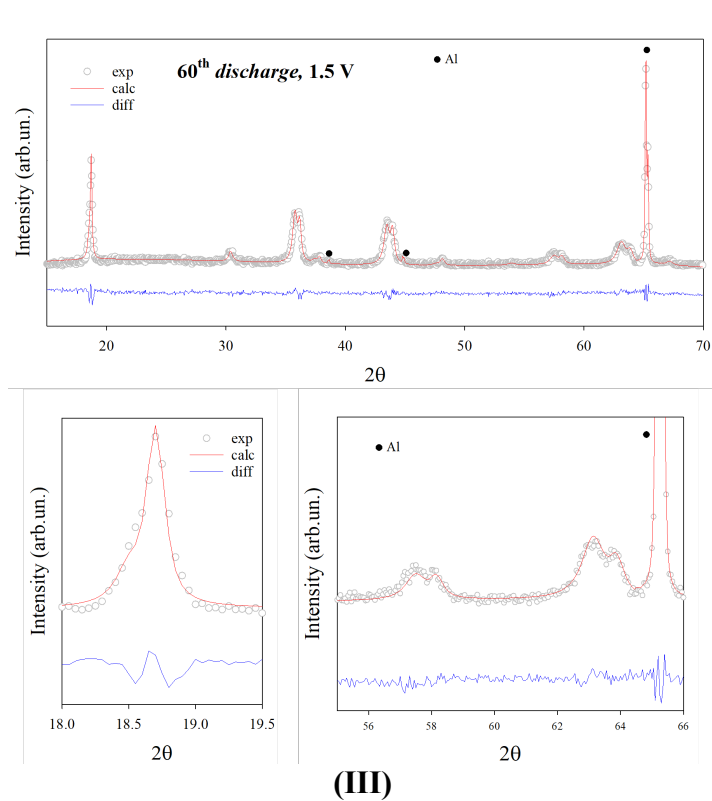


Figure S8: Rietveld refinements of specimen LFMTc discharged at 1.5 V after (I) 5, (II) 10 and (III) 60 electrochemical cycles, plotted full range and zoomed into different regions. Empty dots: experimental data, red solid line: calculated profile, blue solid line: difference curve. Full cycles highlight the signal of the Al support of the electrode.

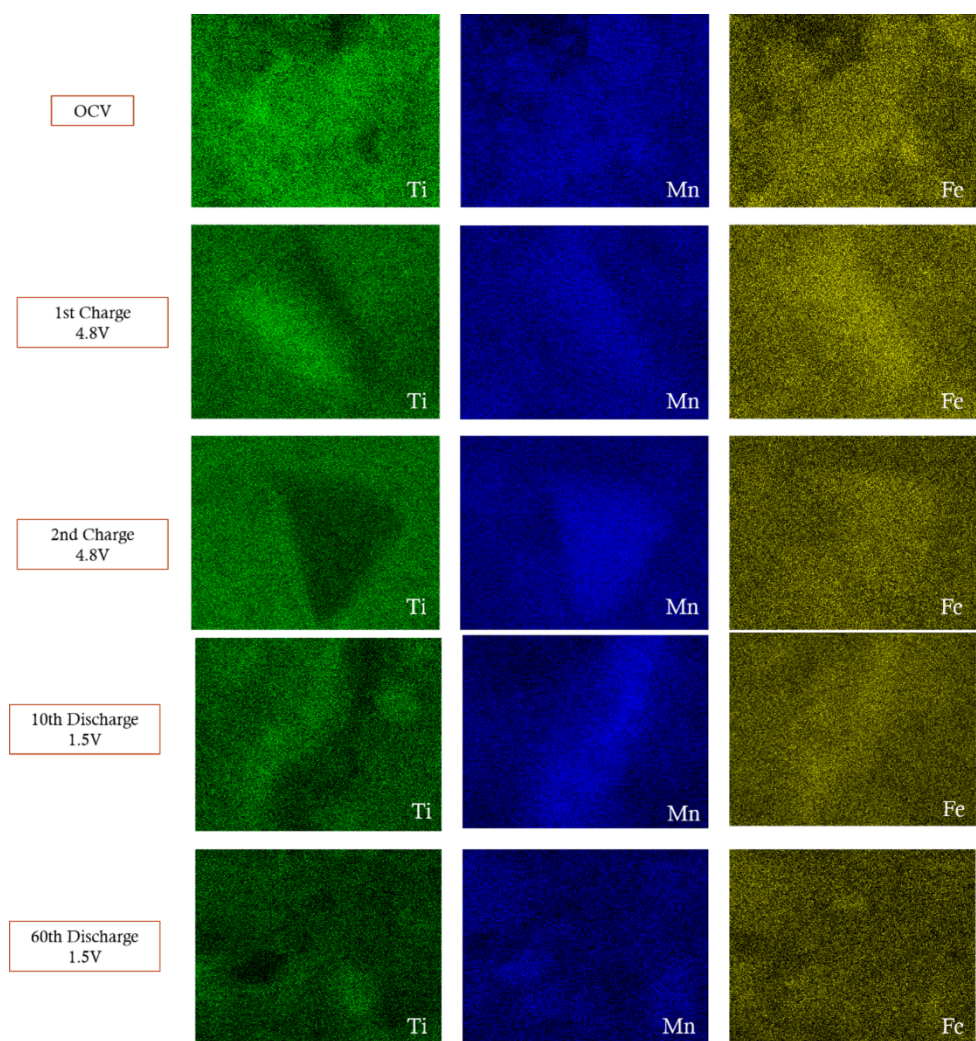


Figure S9: EDX TMs mapping images of the cathodes frozen at OCV, delithiated at 4.8 V and lithiated at 1.5 V at different selected cycles.

	<i>i.r.t</i> (Å)	<i>i.r.o</i> (Å)
Li ⁺	0.59	0.76
Fe ³⁺	0.49	0.645
Mn ³⁺	-	0.645
Mn ⁴⁺	0.39	0.53
Ti ⁴⁺	0.42	0.605
Mn ²⁺	0.66	0.83

Table S1: Ionic radii of the species of interest in tetrahedral (IV) and octahedral (VI) coordination according to Shannon.²

References.

1. Stavitski, E.; De Groot, F. M. F. The CTM4XAS Program for EELS and XAS Spectral Shape Analysis of Transition Metal L edges. *Micron*, 2010, 41, 687– 94.
2. R.D. Shannon, "Revised Effective Ionic Radii and Systematic Studies of Interatomic Distances in Halides and Chalcogenides", *Acta Cryst.* 1976, A32, 751-767.